

The Flight Spectral Response of the ACIS Instrument

Paul P. Plucinsky^a, Norbert S. Schulz^b, Herman L. Marshall^b, Catherine E. Grant^b,
George Chartas^c, Divas Sanwal^c, Marcus A. Teter^c, Alexey A. Vikhlinin^a,
Richard J. Edgar^a, Michael W. Wise^b, Glenn E. Allen^b, Shanil N. Virani^a,
Joseph M. DePasquale^a, and Michael T. Raley^a

^aHarvard-Smithsonian Center for Astrophysics, 60 Garden St., Cambridge, MA 02138

^bCenter for Space Research, Massachusetts Institute of Technology, Cambridge, MA 02139

^cDepartment of Astronomy & Astrophysics, Pennsylvania State University,
University Park, PA 16802

ABSTRACT

We discuss the flight calibration of the spectral response of the *Advanced CCD Imaging Spectrometer* (ACIS) on-board the *Chandra X-ray Observatory* (CXO). The spectral resolution and sensitivity of the ACIS instrument have both been evolving over the course of the mission. The spectral resolution of the frontside-illuminated (FI) CCDs changed dramatically in the first month of the mission due to radiation damage. Since that time, the spectral resolution of the FI CCDs and the backside-illuminated (BI) CCDs have evolved gradually with time. We demonstrate the efficacy of charge-transfer inefficiency (CTI) correction algorithms which recover some of the lost performance. The detection efficiency of the ACIS instrument has been declining throughout the mission, presumably due to a layer of contamination building up on the filter and/or CCDs. We present a characterization of the energy dependence of the excess absorption and demonstrate software which models the time dependence of the absorption from energies of 0.4 keV and up. The spectral redistribution function and the detection efficiency are well-characterized at energies from 1.5 to 8.0 keV primarily due to the existence of strong lines in the ACIS calibration source in that energy range. The calibration at energies below 1.5 keV is challenging because of the lack of strong lines in the calibration source and also because of the inherent non-linear dependence with energy of the CTI and the absorption by the contamination layer. We have been using data from celestial sources with relatively simple spectra to determine the quality of the calibration below 1.5 keV. We have used observations of 1E0102.2-7219 (the brightest supernova remnant in the SMC), PKS2155-304 (a bright blazar), and the pulsar PSR 0656+14 (nearby pulsar with a soft spectrum), since the spectra of these objects have been well-characterized by the gratings on the CXO. The analysis of these observations demonstrate that the CTI correction recovers a significant fraction of the spectral resolution of the FI CCDs and the models of the time-dependent absorption result in consistent measurements of the flux at low energies for data from a BI (S3) CCD.

Keywords: CXO, Chandra, ACIS, Charge-Coupled Devices, CCDs, X-ray detectors, X-ray spectroscopy

1. INTRODUCTION

The Chandra X-ray Observatory (CXO) is the third of NASA's great observatories in space.^{1,2} The CXO was launched just past midnight on July 23, 1999 aboard the space shuttle *Columbia* on the STS-93 mission. The CXO was placed into a higher orbit by an Inertial Upper Stage (IUS) booster and then used its own propulsion system to achieve a final orbit with a perigee of 10,000 km, an apogee of 140,000 km, an inclination of 28.5° and a period of ~ 64 hr. The CXO is controlled and operated by the Smithsonian Astrophysical Observatory (SAO) from Cambridge, Massachusetts. The Chandra X-ray Center (CXC), also run by the Smithsonian Astrophysical Observatory, processes and distributes Chandra data and provides analysis software and calibration products to the astronomical community.

Further author information: (Send correspondence to P.P.P.)

P.P.P.: E-mail: plucinsky@cfa.harvard.edu, Telephone: 1 617 496 7726

The CXO carries two focal plane science instruments: the *Advanced CCD Imaging Spectrometer* (ACIS) and the *High Resolution Camera* (HRC). The Observatory also possesses two objective transmission gratings: a *Low Energy Transmission Grating* (LETG) that is primarily used with the HRC, and the *High Energy Transmission Grating* (HETG) that is primarily used with the ACIS. ACIS was developed by a team from the Massachusetts Institute of Technology³ and the Pennsylvania State University⁴ and is the primary scientific instrument aboard CXO, currently conducting $\sim 90\%$ of the observations. It contains two arrays of CCDs, one optimized for imaging and the other for spectroscopy as the readout detector for the HETG. The ACIS imaging array contains 4 Front-Illuminated (FI) CCDs configured in a 2×2 array and the spectroscopy array contains 2 Back-Illuminated (BI) CCDs and 4 FI CCDs configured in a 1×6 array.

2. THE TIME EVOLUTION OF THE SPECTRAL RESPONSE

The spectral response of the ACIS CCDs has been evolving with time since the launch of CXO due to an increase in the charge-transfer inefficiency (CTI) and the development of a contamination layer on the filter and/or the CCDs. The CTI introduces a spatial dependence in the spectral resolution of the detectors. The contamination layer introduces an energy-dependent reduction in the detection efficiency of the instrument. The relative importance of these effects are different for the FI and BI CCDs. We discuss these effects in detail in the following sections and also discuss the the low-energy gain and spectral redistribution function of the BI CCDs.

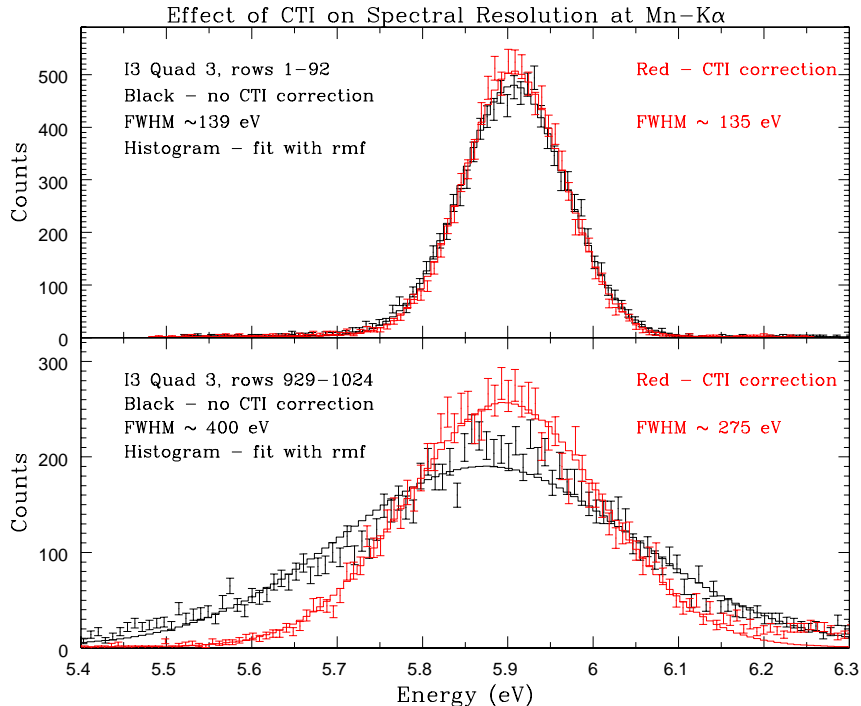


Figure 1. Comparison of PH distributions from Mn $K\alpha$ X-rays (5.9 keV) from the ACIS external calibration source with and without a CTI correction. The top panel displays the PH distribution from the bottom of the CCD where the effects of CTI are minimal. The bottom panel displays the PH distribution from the top of the CCD where the effects of CTI are at a maximum.

2.1. RADIATION DAMAGE AND CHARGE TRANSFER INEFFICIENCY

In the first month of the mission, the FI CCDs on ACIS suffered a large increase in CTI^{5,6} (CTI is defined as the fractional charge loss per pixel transferred). The CTI increased from essentially zero to $\sim 1.0 - 2.0 \times 10^{-4}$. The CTI varies from CCD to CCD as the FI CCDs in the imaging array were less damaged than the FI CCDs in the spectroscopy array. The BI CCDs showed no measurable increase in CTI during this time frame. During

the first month of the mission, ACIS was left at the focus of the telescope during the radiation belt transits. It is believed that the damage was the result of low-energy protons ($\sim 100 - 200$ keV) which scattered off of the CXO's mirrors with a sufficient efficiency to produce a significant flux at the focal plane. The ACIS instrument is now moved out of the focal position of the telescope during every radiation belt transit and the rapid increase in CTI has not continued. The CTI of both the FI and BI CCDs has been slowly increasing over the remaining three years of the mission. This gradual increase is presumably the result of the accumulated damage of high-energy protons which penetrate the ACIS proton shield and residual low-energy protons which are encountered outside of the radiation belts.

The ACIS CCDs are framestore design CCDs. The CCD consists of an imaging array and a framestore array. The imaging array is exposed to the incident radiation and the framestore array is covered by an Al shield. The framestore cover is sufficiently thick to stop the low-energy protons which produce the increase in CTI. Therefore, the CTI of the framestore array in the FI CCDs is unchanged since launch and is still essentially zero. Figure 1 displays the effect of CTI on a pulse-height (PH) distribution generated from Mn $K\alpha$ X-rays from the ACIS external calibration source in flight on the I3(FI) CCD. The top panel shows the PH distribution from rows 1-92 of the CCD near the framestore array and the bottom panel shows the PH distribution from rows 929-1024 near the top of the CCD. Since only the parallel CTI in the imaging array increased and the parallel and serial CTI in the framestore array remained unchanged, the problem was reduced to one dimension in row number on the CCD. It was possible to construct an algorithm which compensated for the charge lost to CTI on an event-by-event basis which improves the resulting spectral resolution.^{7,8} The correction software recovers some, but not all, of the lost performance. In Figure 1, we have plotted the PH distributions after the CTI correction software (SW) has been applied to the data. Note that the correction modifies the data only slightly near the framestore region, but modifies the data significantly near the top of the CCD. The correction algorithm improves the spectral resolution by $\sim 30\%$ at the top of the CCD.

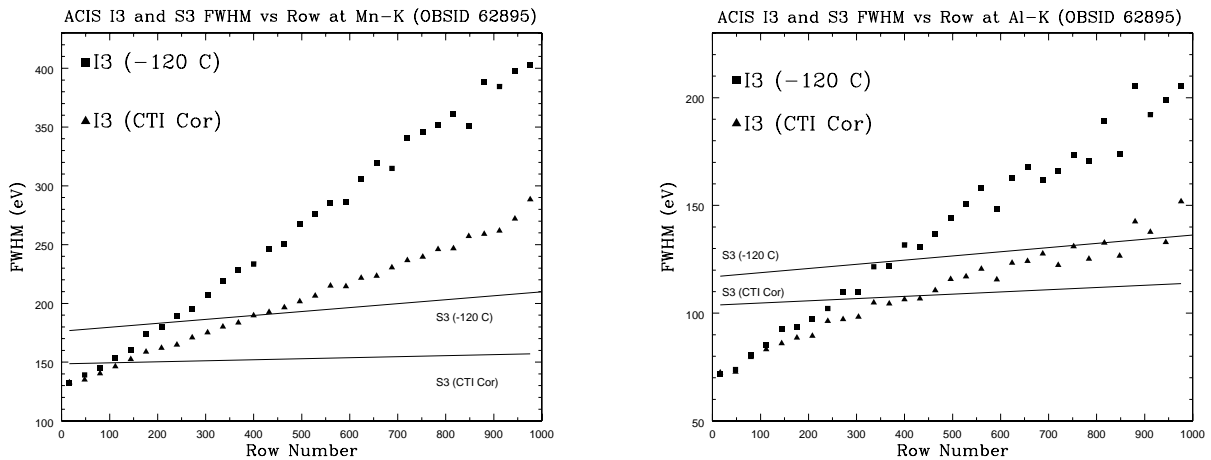


Figure 2. The FWHM of the ACIS I3 detector versus row number with and without a CTI correction for Mn $K\alpha$ X-rays (5.9 keV) (LEFT) and Al $K\alpha$ X-rays (1.5 keV) (RIGHT). Complementary numbers for the S3 detector are plotted for reference.

We have analyzed the data from a long observation under the ACIS external calibration source (OBSID 62895) to determine the variation of the full-width at half maximum (FWHM) versus row number. We have conducted this analysis with the uncorrected data and the CTI-corrected data. Figure 2 displays the FWHM versus row number for Mn $K\alpha$ X-rays and for Al $K\alpha$ X-rays for the I3(FI) CCD. The CTI correction provides a significant improvement at both energies. We have also plotted the FWHM versus row number for the S3 CCD for comparison. After applying the CTI correction, the FI CCDs in the ACIS imaging array provide better spectral resolution than S3 over the bottom half of the CCD at 1.5 keV.

We have used an implementation of the CTI corrector developed by the CXC for a future release of the *Ciao* SW for the I3 data and have used the publicly available CTI correction SW from the Penn State group for the

S3 data. We have compared the I3 results from the CXC CTI corrector and the Penn State CTI corrector and found the results to be nearly identical. The CTI correction SW is available from the Penn State group at the CXC contributed SW web site:

<http://asc.harvard.edu/cont-soft/software/ACISctiCorrector.1.37.html>.

2.2. CONTAMINATION BUILDUP AND LOW-ENERGY DETECTION EFFICIENCY

It was noticed in early 2002 that the detection efficiency of the ACIS instrument had been declining gradually over the life of the mission. The effect at energies above 1.5 keV is negligible, but the effect at lower energies is large ($\sim 50\%$ reduction in quantum efficiency at 0.5 keV over the first three years of the mission). The ACIS external calibration source produces weak Mn L and Fe L lines in addition to the Mn K lines. We have analyzed the ratio of the Mn L complex and Mn K lines over the life of the mission. The data are plotted in Figure 3 and indicate the ratio has been decreasing throughout the mission. The rate of decrease appears to be slowing with time. The data have been fit with a function of the form⁹:

$$\text{Mn L/Mn K ratio} = N_o \times \exp[-\tau_\infty \times (1 - \exp(-t/\tau_o))] \quad (1)$$

where N_o is the value of the ratio at $t = 0$, t is the number of days since launch, τ_∞ is the value of the optical depth at $t = \infty$, and τ_o is a characteristic time constant. Since this function is an exponential of an exponential decay in time, we cannot interpret the value of τ_o as the characteristic time constant of the overall decay. The asymptotic value of this function is 0.00403. If this model can be legitimately extrapolated into the future, this implies that $\sim 80\%$ of the decrease in the ratio has already occurred.

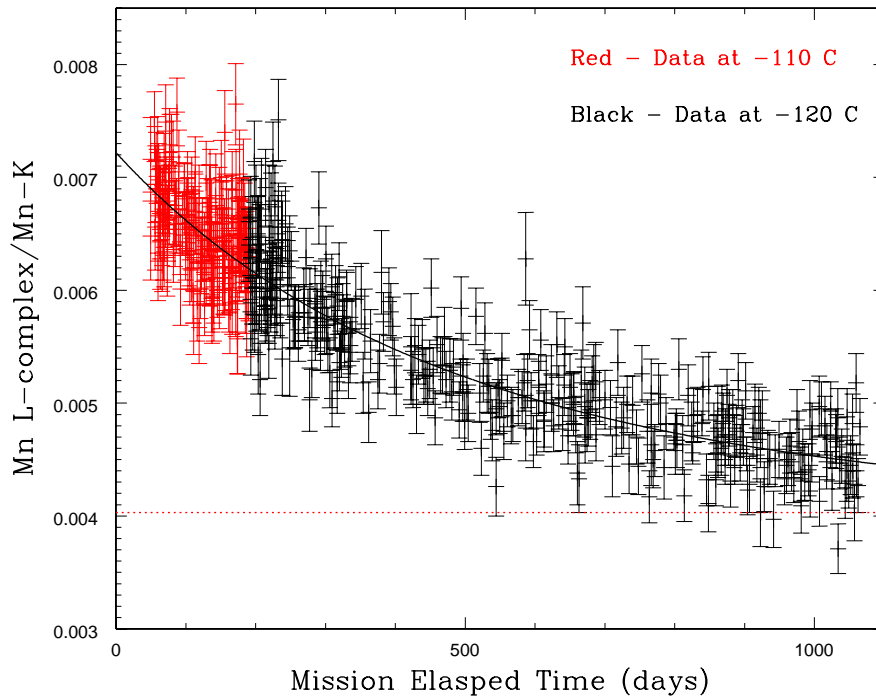


Figure 3. The ratio of the Mn L/Fe L complex/Mn K lines versus time from the S3(BI) CCD. The data collected with the focal plane at -110 C are indicated in red and the data collected at -120 C are indicated in black. The solid line is a model of the time dependence in Eqn. 1 and the red dashed line is the asymptotic value of 0.00403.

Once the putative contamination layer was discovered in early 2002, a series of calibration observations were conducted to better characterize the nature of the contamination. Several observations were conducted

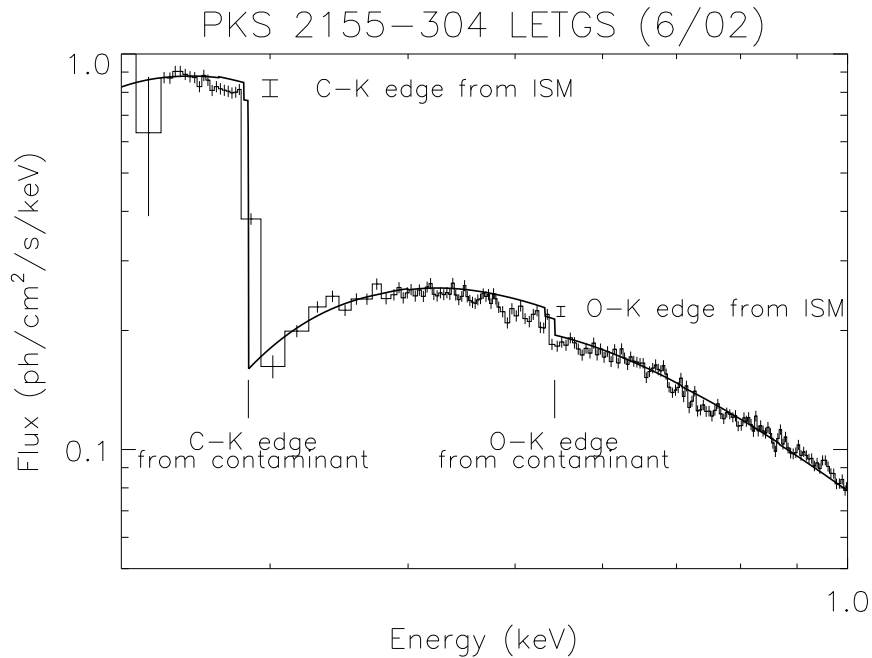


Figure 4. The ACIS LETG spectrum of PKS2155 from OBSID 3669. The C and O absorption edges from the ISM and the contaminant are identified.

in the LETG/ACIS configuration to provide a well-characterized spectrum with a large flux of low energy photons. Figure 4 displays the LETG/ACIS spectrum from OBSID 3669, an 45ks observation of the bright blazar PKS2155-304.

The spectrum of PKS 2155-304 was fit with two power-law components absorbed by neutral gas in the Galactic ISM using the abundances and opacities of Wilms *et al.*¹⁰ The C-K and O-K edges due to the contaminant were fit to the data, giving optical depths of 1.58 ± 0.02 and 0.10 ± 0.01 , respectively. Residuals of $\sim 5\%$ near 0.5 keV probably result from a poor model of the transmission of the contaminant. There is no detection of a N-K edge and the 90% upper limit to the optical depth there is about 0.04. Residuals near 0.7 keV may result from fluorine in the contaminant but there is no clear edge nor is there a good model of the absorption due to fluorine in relevant compounds.

Since the contamination layer is composed mostly of C, the largest effect on CXO data will be at energies below 1.0 keV. We have examined calibration observations of 1E0102.2-7219, the brightest supernova remnant in the Small Magellanic Cloud which has a soft, line-dominated spectrum. Figure 5 displays four observations of 1E0102.2-7219 separated by two years in time. The bottom panel of the plot displays the difference between the earliest and latest observation. It is clear from these data that the largest effects occur at energies below 1.5 keV. It is also clear that the data above 1.5 keV are mostly unaffected.

2.3. LOW-ENERGY GAIN AND SPECTRAL REDISTRIBUTION FUNCTION FOR THE BI CCDS

We have reported previously on our efforts to improve the response model of the BI CCDs on ACIS.¹¹ For a thorough discussion of the models developed for the ACIS CCDs, the reader is referred to the publications by the ACIS team.^{12,13} The model of the spectral redistribution function for the S3 response matrix was significantly improved in the release of the CXO calibration database CALDB2.7. At that time we noted that the gain and the redistribution function were well-modeled above 0.8 keV, but that there were still deficiencies below 0.8 keV. We have used the observations of PKS2155-304 with the LETG to investigate the response of the S3 CCD. The advantage of the LETG data is that the energy of the incident photons can be determined from their position on the CCD and can therefore be used to verify the conversion from pulse height to energy.

Comparison of E0102 Observations on S3

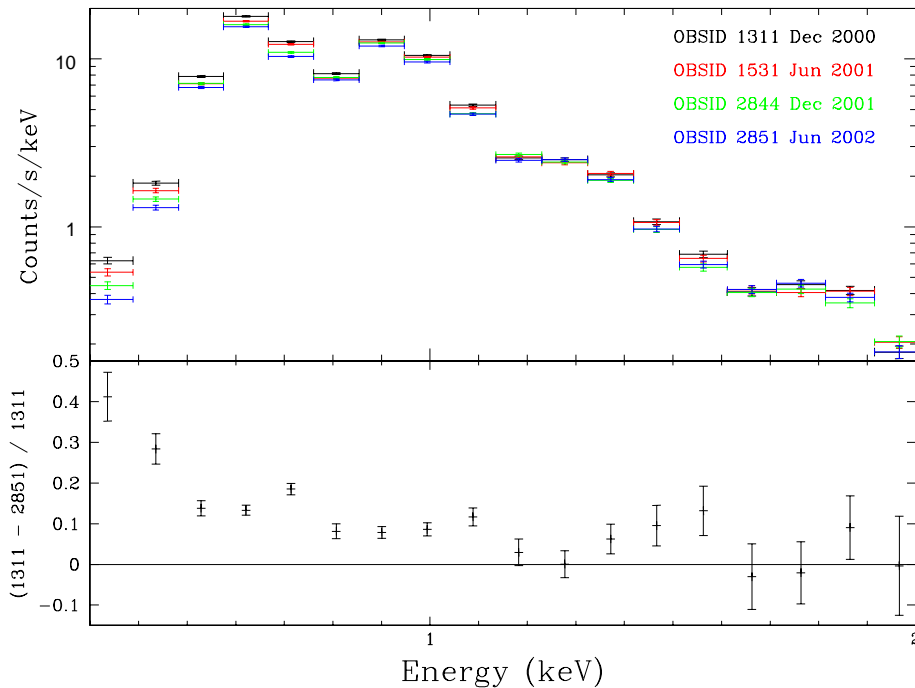


Figure 5. S3(BI) observations of E0102 at different epochs, different epochs are indicated by different colors. The data have been binned into relatively large bins in energy space to provide a statistically significant number of counts in each bin. The bottom panel shows the fractional difference between the earliest and latest observations.

By using pointing offsets in multiple observations, we have been able to acquire a range of energies at the same location on the CCD. These data can then be used to characterize the gain and spectral redistribution function at low energies.

We have used the data from OBSIDs 2323, 2324, and 3669 to investigate the gain at low energies. OBSIDs 2323 and 2324 positioned the dispersed spectrum from the LETG at the nominal readout location in the middle of the CCD and OBSID 3669 positioned the dispersed spectrum closer to the framestore region using a translation offset in the Science Instrument Module (SIM). Figure 6 plots the ratio of the energy determined from the PH of the event to the energy determined by the dispersion relation of the LETG. The energy determined from the PH of the event agrees with the LETG-determined energy to within $\pm 2\%$ near the readout. However, the data near the aimpoint show a systematic offset of 2–6% for energies below 900 eV with the CCD PH overestimating the true energy of the photon. We will be able to use the multiple calibration observations of PKS2155-304 to refine the low-energy gain of the S3 CCD as a function of position to be incorporated in an updated matrix of the CXO CALDB. It is important to emphasize the energy of the events as determined by the PH agrees with the LETG-determined energy at both locations for energies above 0.9 keV.

The PKS2155-304 LETG/ACIS data are also useful for investigating the model of the spectral redistribution function. Once again, we can restrict our analysis to a very narrow range of energies by selecting events by position on the CCD. We have extracted data from the location on the CCD which corresponds to an energy of ~ 0.65 keV and ~ 0.97 keV and fit these data with the existing response matrix for S3. The data and model fits are displayed in Figure 7. The low-energy side of the 0.65 keV peak is not well represented by the existing model. It is clear that the model overestimates the contribution of the tail. The 0.97 keV data are well-fitted by the model, both the peak and the low energy tail. We will be able to use the multiple calibration observations of PKS2155-304 to refine the spectral redistribution model of the S3 CCD at low energies to be incorporated in an updated matrix of the CXO CALDB. These data verify that the spectral redistribution function is well-represented by the existing matrix for energies above 0.9 keV.

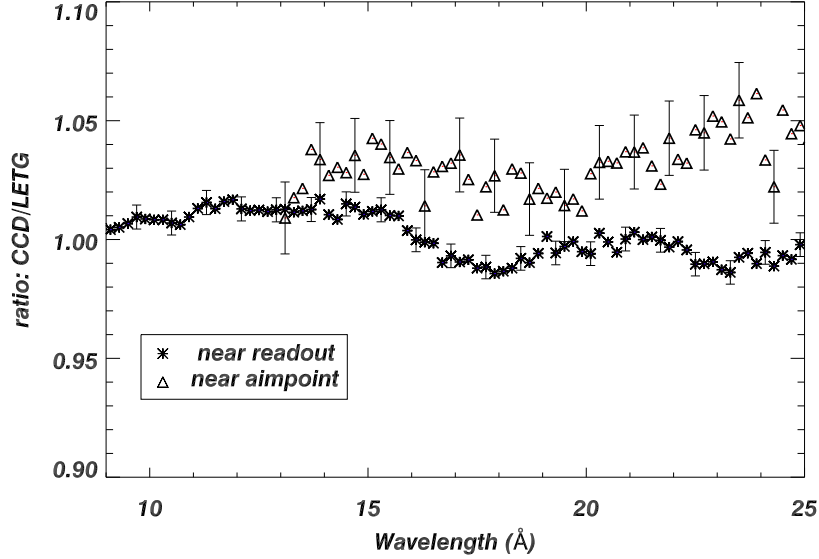


Figure 6. Evaluation of the low-energy gain of the S3 CCD. The ratio of the energy determined by the PH of the event and the energy determined by the dispersion of the LETG is plotted versus wavelength. Two locations on the CCD are plotted, one near the aimpoint (OBSIDs 2323 & 2324) and one near the framestore (OBSID 3669) in chip row number.

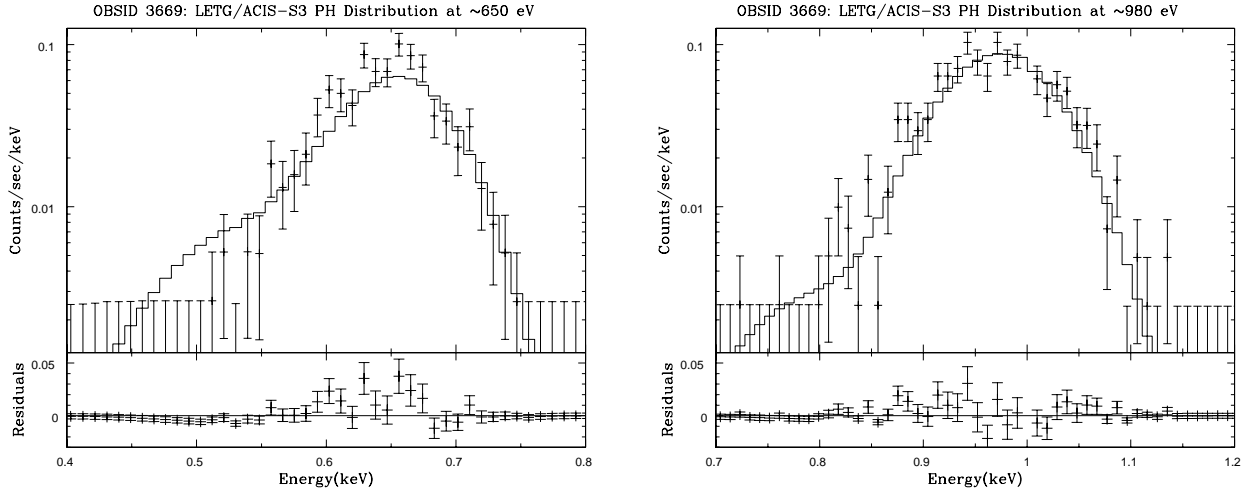


Figure 7. The PH distributions extracted from the region of the CCD corresponding to energies from 0.636 to 0.670 keV (LEFT) and 0.943 to 1.021 keV (RIGHT) from the LETG/ACIS observation of PKS2155-304 (OBSID 3669). The tail of the spectral redistribution is not well-represented for energies around 650 eV but is well represented for energies above 0.90 keV.

3. APPLICATIONS TO CELESTIAL SOURCES

We have been evaluating the calibration products using a variety of celestial sources. Since the contamination is on the filter and/or CCDs, CXO observations with and without the gratings are affected. We have used 1E0102.2-7219 because it has a soft, line-dominated spectrum which has been well-characterized by the gratings on the CXO¹⁴ and *XMM-Newton*.¹⁵ We have developed a spectral model based on the lines observed in the gratings data which contains 24 Gaussians for the lines, a two component absorption (one for the Galactic component and one for the SMC), and a bremsstrahlung for the continuum. As mentioned in the earlier sections,

we have used the bright blazar PKS2155-304 which, even though the intensity and spectral shape vary in time, can be well-modeled by absorption plus a two component power-law. We have also used the galactic SNR G21.5-0.9 which has a heavily-absorbed power-law spectrum.¹⁶ Finally, we have used the pulsar PSR 0656+14 which has a soft, continuum spectrum.

There are two SW tools which have been developed to model the time-dependent effect of the absorption by the contamination layer. One is an XSPEC model, which would be used as an additional multiplicative component while fitting in XSPEC (version 11.2 or above) or SHERPA and is called ACISABS. The other is a stand-alone program written in IDL and FORTRAN called ACISABS.pro and corr_arf, respectively, that modifies the effective area values in the arf file. The ACISABS tools calculate the transmission through the contamination layer assumed to consist of a hydrocarbon of the form $C_{n1}, H_{n2}, O_{n3}, N_{n4}$, where, $n1, n2, n3$ and $n4$ are input parameters and represent the number of atoms of the respective element in the hydrocarbon molecule. The mass absorption coefficients of the contaminant are calculated from the atomic scattering factor files provided at “http://www-cxro.lbl.gov/optical_constants/asf.html”. Both of these SW tools are available from the CXC contributed SW page: “<http://asc.harvard.edu/cont-soft/soft-exchange.html>”. The results of this paper have made use of the corr_arf program which assumes that C, H, N, and O are present in the contamination layer in the ratio of 10:20:1:2, respectively. The composition of the contaminant will probably need to be updated when the nature of the contaminant is better constrained with future observations.

The SW to correct events list for CTI is also available from the CXC contributed SW page. It currently exists in the form of IDL code which the user must install at their site. The CXC has been implementing the CTI correction in the standard processing of the *Ciao* SW to be released in a future version. For this paper, we have used a development version of the *Ciao* SW which includes the CTI correction algorithm.

3.1. G21.5-0.9: HARD, CONTINUUM SOURCE

As a first example, we present a source with a hard continuum spectrum for which the fitted results do not vary significantly because of the absorption by the contamination layer. We have fit three observations of G21.5-0.9 separated by over a year with and without the effective area correction. All of these observations are on the S3 CCD near the nominal aimpoint. We fit the data with an absorption plus power-law model. Unfortunately, the ACIS configuration was different for the observations. OBSID 1717 used a full-frame readout with a frametime of 3.2 s and OBSIDs 1553 and 1554 used a frametime of 0.8 s with a subarray readout. Therefore, the pileup will be different in the observations. The results and the 90% confidence limits (CL) in Table 1 indicate that there is a negligible difference between the fit with and without the effective area correction for all three observations. Therefore, any spectral results derived from ACIS before July 2001 from a source with a hard, continuum spectrum such as that of G21.5-0.9 will change by less than 2% when the effective area correction is applied. The derived flux values for the observations with the shorter frametime are $\sim 4\%$ higher, as one would expect if the pileup were reduced in these observations.

Table 1. Spectral Fit Results for G21.5-0.9 with and without the effective area correction

OBSID	DATE	E.A. Cor.	Frm Tim (s)	$N_H(10^{22} \text{ cm}^{-2})$	Power-law Index	Norm @ 1 keV ($\times 10^{-2}$) (photons /keV/cm ² /s)	Flux ($\times 10^{11}$) [0.5-9.0 keV] (ergs/cm ² /s)
1717	2000-05-23	No	3.2	2.25 [2.18,2.32]	1.84 [1.78,1.89]	2.02 [1.87,2.18]	5.33
1717	2000-05-23	Yes	3.2	2.22 [2.15,2.29]	1.83 [1.78,1.89]	2.01 [1.86,2.17]	5.34
1553	2001-03-18	No	0.8	2.28 [2.22,2.34]	1.86 [1.81,1.90]	2.18 [2.04,2.33]	5.55
1553	2001-03-18	Yes	0.8	2.23 [2.17,2.29]	1.85 [1.81,1.90]	2.16 [2.02,2.31]	5.58
1554	2001-07-21	No	0.8	2.23 [2.18,2.30]	1.82 [1.78,1.87]	2.06 [1.92,2.21]	5.54
1554	2001-07-21	Yes	0.8	2.18 [2.12,2.25]	1.82 [1.77,1.87]	2.04 [1.91,2.19]	5.57

3.2. 1E0102.2-7219: SOFT, LINE-DOMINATED SOURCE

For a source with a soft, line-dominated spectrum, the effective area correction makes a large difference. We fit the four observations of 1E0102.2-7219 shown in Figure 5 which show dramatic differences at the lowest

energies. These observations used the S3 detector and were within 0.5 arcminute of the on-axis aimpoint. The spectrum is dominated by strong lines of O and Ne. We determined the flux in the O VIII Ly α , Ne IX triplet, and the Ne X Ly α lines in each of the four observations, in addition to the best-fit values for the N_{H} and kT . The results with the 90% CL are presented in Figure 8. The N_{H} values for OBSIDs 1311 and 1531 are in good agreement with estimates from optical measurements. However, the N_{H} values for OBSIDs 2844 and 2851 are significantly higher. It is not clear if this is because the absorption from the contamination layer has been underestimated as a function of time or if a change in the detector response with time could mimic an excess N_{H} . The fitted values for the temperature and the line fluxes are in agreement over this two year period. There is a hint that the increase in the derived flux for the O VIII Ly α line might be correlated with the increase in the derived value of the N_{H} , but the fluxes agree within the 90% CL. The derived fluxes for the Ne lines are in agreement with each other for all four observations.

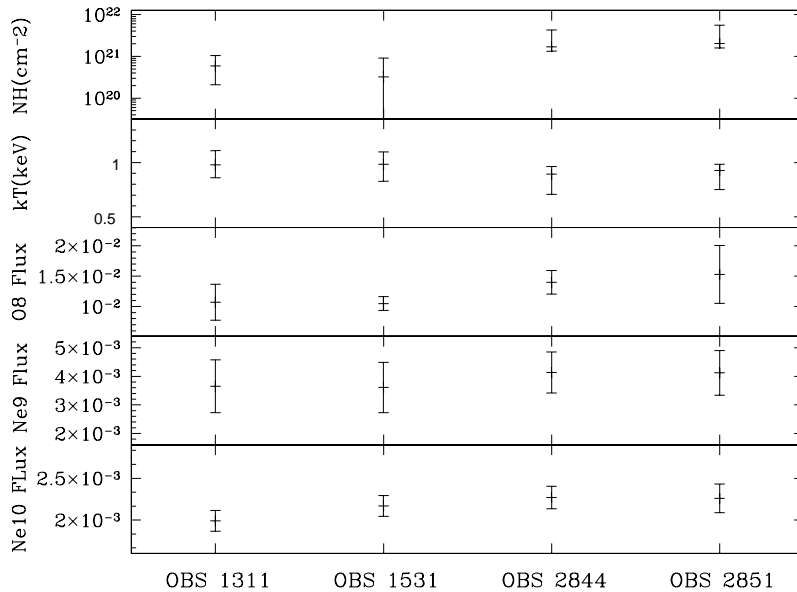


Figure 8. Spectral results from E0102 from the S3(BI) CCD for four observations spanning two years after applying the effective area correction. The line fluxes are in units of photons $\text{cm}^{-2} \text{s}^{-1}$.

3.3. PSR0656+14: SOFT, CONTINUUM SOURCE

We have also fit the spectrum of the nearby pulsar PSR 0656+14. This source has a very soft spectrum which is only slightly modified by the intervening interstellar medium. ACIS was operated in continuous-clocking (CC) mode for this observation. Pavlov *et al.* (2002)¹⁷ have fit the spectrum with a three component model consisting of two blackbody components and a power-law component. Marshall & Schulz (2002)¹⁸ analyzed the HRC/LETG spectrum of PSR 0656+14, which is unaffected by the contamination layer and also provides the highest resolution spectral data acquired for this object, and derived parameters for the two blackbody components which are consistent with the ACIS CC mode results. We fit the spectrum with and without the effective area correction. Figure 9 displays the best fit with the effective area correction and the same model folded through the default effective area curve. The temperatures of the blackbody components changed little between the fits but the normalizations changed significantly, leading to a large difference in the derived flux. The fitted values of the flux of these two fits are shown in Table 2. We have restricted the fit to energies from 0.4 keV to 5.0 keV due to the uncertainties in the low-energy response of ACIS below 0.4 keV but we have computed the flux from 0.24 keV to 3.0 keV to compare to previous results. These results demonstrate that the derived flux can be different by as much as a factor of three for a soft, continuum spectrum.

Table 2. Spectral Fit Results for PSR 0656+14 with and without the effective area correction

Effective Area Correction	Flux [0.24-3.0 keV] (ergs/cm ² /s)
No	0.70×10^{11}
Yes	2.60×10^{11}

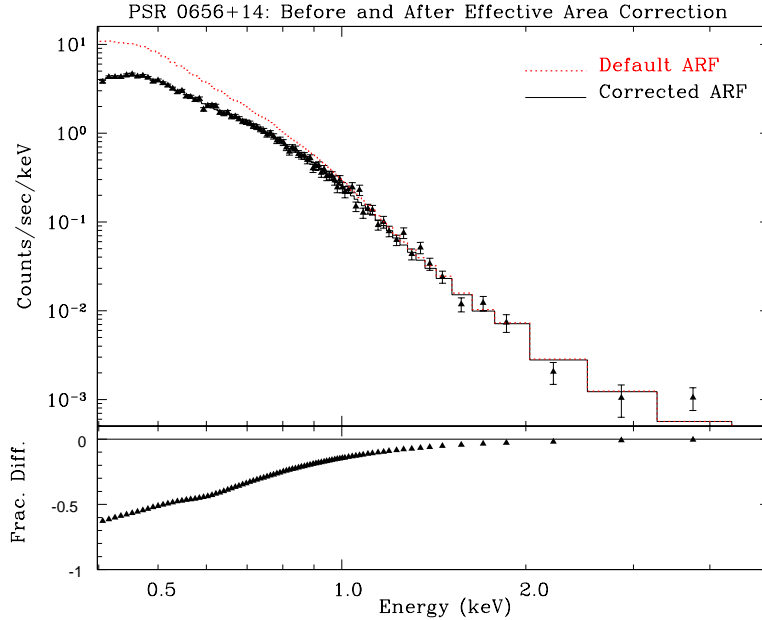


Figure 9. Spectrum of PSR0656+14 with the best-fit spectrum with the corrected effective area plotted in black. This model is then folded through the default effective area curve (plotted in red) and the difference of the two models is plotted in the lower panel.

3.4. 1E0102.2-7219: CTI CORRECTION

Five observations of 1E0102.2-7219 were executed at different `chipy` locations on the I3 CCD from near the nominal aimpoint to the framestore region. The spacing between observations was ~ 150 rows. We have analyzed these observations to investigate the performance of the CTI correction algorithm at low energies as the source is moved across the CCD. We fit these data with the same model described earlier. We applied both the CTI correction and the effective area correction to the I3 observations. Three of the five spectra are plotted in Figures 10 and 11. The three observations which are plotted are OBSIDs 420, 136, and 440, which are closest to the framestore, in the middle of the CCD, and closest to the aimpoint respectively. The spectrum for OBSID 420 exhibits spectral resolution at nearly the pre-launch, undamaged value. Notice how the O VII triplet is resolved from the O VIII Ly α line and the Ne IX triplet is resolved from the Ne X Ly α line. OBSID 136 demonstrates the spectral resolution available in the middle of the CCD. The lines have clearly started to blend together. Finally, OBSID 440 demonstrates the resolution available at the top of the CCD. Similar to the exercise for 1E0102.2-7219 on S3, we have determined the fitted parameters of the N_{H} , kT, O VIII Ly α line flux, the Ne IX triplet flux and the Ne X Ly α line flux for these five observations. The values are plotted versus OBSID in Figure 11. There is excellent agreement among the observations for all the fitted parameters except for the N_{H} and kT for OBSID 140. These results demonstrate that after applying the CTI correction and the effective area correction, consistent results can be achieved for a source with a soft, line-dominated spectrum as a function of time on the I3 CCD.

3.5. CONCLUSIONS

The flight spectral response of the ACIS instrument is well-characterized in the 1.5 keV to 8.0 keV bandpass. The current calibration products provide for consistent results between observations of the same source at

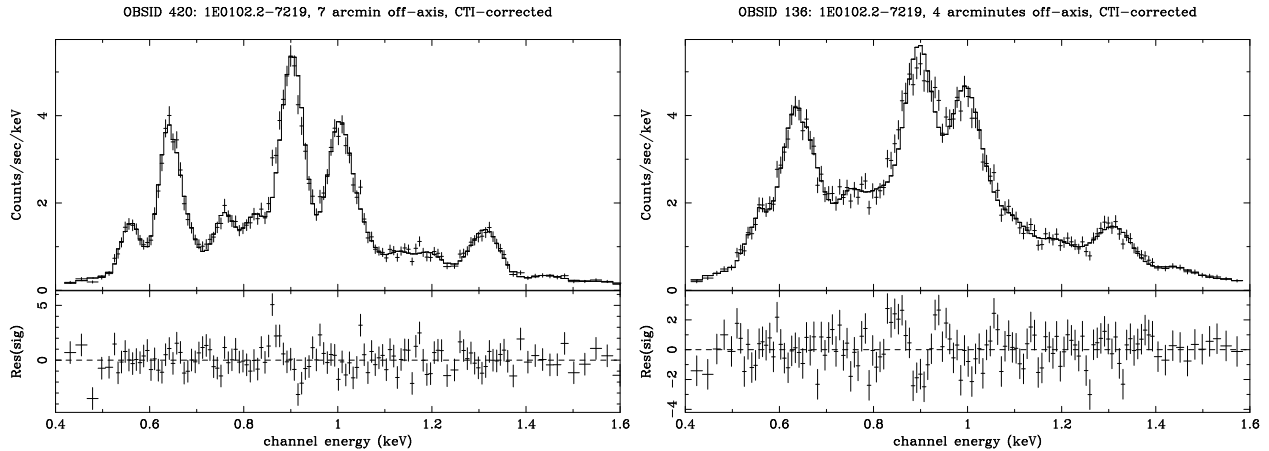


Figure 10. Spectra of 1E0102.2-7219 extracted from the I3 CCD from near the framestore (LEFT) OBSID 420 and in the middle of the CCD (RIGHT) OBSID 136. The CTI correction and the effective area correction have been applied.

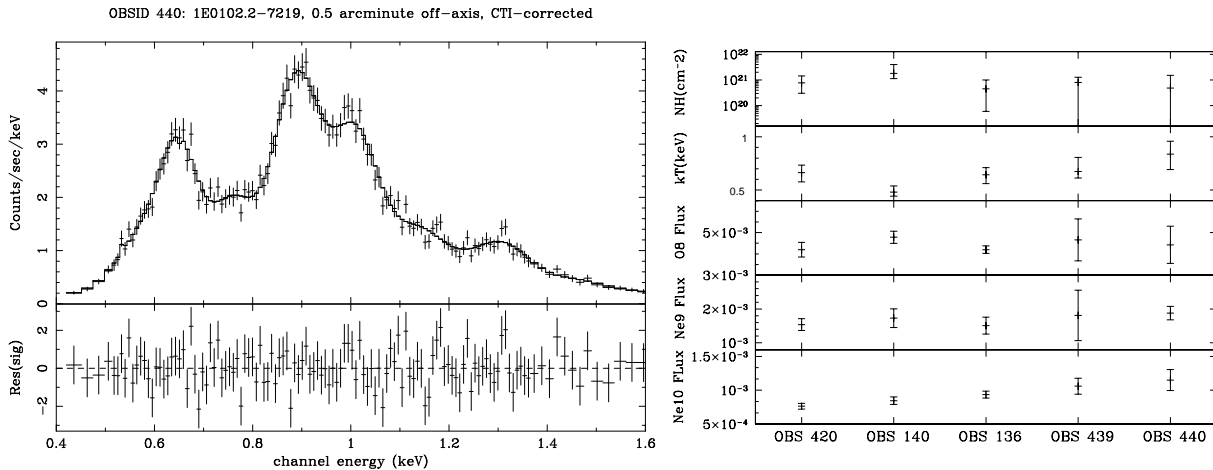


Figure 11. (LEFT) Spectrum of 1E0102.2-7219 extracted from the I3 CCD from near the aimpoint OBSID 440. (RIGHT) The derived values from the fits of the five observations which span the I3 CCD. There is excellent agreement among the observations after the CTI correction has been applied and the effective area correction.

different epochs and at different detector positions within the measurement uncertainties. The uncertainties in the calibration below 1.5 keV are significantly larger and are dominated by the temporal variation of the spectral resolution and the detection efficiency. The level of uncertainty depends strongly upon the spectral shape of the source and the precise energy of interest. We have demonstrated that the application of a time-dependent effective area correction and a CTI correction improve significantly the consistency of the results below 1.5 keV.

ACKNOWLEDGMENTS

This work was supported by NASA contract NAS8-39703.

We thank many of our colleagues on the CXO project who have contributed directly or indirectly to this work. We thank Mark Bautz, Bev LaMarr, Peter Ford, Dan Schwartz, Leisa Townsley, George Pavlov, Konstantin Getman, Martin Weisskopf, Steve O'Dell, Allyn Tennant, Ron Elsner and all members of the ACIS instrument team and CXO Project Science who have contributed to this effort. We thank Slava Zavlin for granting us permission to use the observation of PSR0656+14 which is still proprietary at this time. For anyone we have forgotten, we apologize.

REFERENCES

1. M. C. Weisskopf, H. D. Tananbaum, L. P. Van Speybroeck, and S. L. O'Dell, "Chandra x-ray observatory (cxo): overview," in *X-Ray Optics, Instruments, and Missions III*, J. E. Truemper and B. Aschenbach, eds., *Proc. SPIE* **4012**, p. 2, 2000.
2. M. C. Weisskopf, B. Brinkman, C. Canizares, G. Garmire, S. Murray, and L. P. Van Speybroeck, "An overview of the performance and scientific results from the chandra x-ray observatory," *Publications of the Astronomical Society of the Pacific* **114**, p. 1, jan 2002.
3. M. Bautz, M. Pivovarov, F. Baganoff, T. Isobe, S. Jones, S. Kissel, B. Lamarr, H. Manning, G. Prigozhin, G. Ricker, J. Nousek, C. Grant, K. Nishikida, F. Scholze, R. Thornagel, and G. Ulm, "X-ray ccd calibration for the axaf ccd imaging spectrometer," in *X-Ray Optics, Instruments, and Missions*, R. B. Hoover and A. B. W. II, eds., *Proc. SPIE* **3444**, p. 210, 1998.
4. G. Garmire, G. Ricker, M. Bautz, B. Burrows, D. Burrows, S. Collins, J. Doty, K. Gendreau, D. Lumb, and J. Nousek, "The axaf ccd imaging spectrometer," in *American Institute of Aeronautics and Astronautics Conference*, p. 8, 1992.
5. G. Prigozhin, S. Kissel, M. Bautz, C. Grant, B. LaMarr, R. Foster, G. Ricker, and G. Garmire, "Radiation damage in the chandra x-ray ccds," in *X-Ray Optics, Instruments, and Missions*, J. E. Truemper and B. Aschenbach, eds., *Proc. SPIE* **4012**, p. 720, 2000.
6. G. Prigozhin, S. Kissel, M. Bautz, C. Grant, B. LaMarr, R. Foster, and G. Ricker, "Characterization of the radiation damage in the chandra x-ray ccds," in *X-Ray Optics, Instruments, and Missions*, K. A. Flanagan and O. H. Siegmund, eds., *Proc. SPIE* **4140**, p. 123, 2000.
7. L. K. Townsley, P. S. Broos, G. P. Garmire, and J. A. Nousek, "Mitigating charge transfer inefficiency in the chandra x-ray observatory advanced ccd imaging spectrometer," *Astrophysical Journal* **534**, pp. L139–LL142, 2000.
8. L. K. Townsley, P. S. Broos, J. A. Nousek, and G. P. Garmire, "Modeling charge transfer inefficiency in the chandra advanced ccd imaging spectrometer," *Nuclear Instruments and Methods* **486**, p. 751, 2002.
9. S. O'Dell and A. Tennant *private communication*, 2002.
10. J. Wilms, A. Allen, and R. McCray, "On the absorption of x-rays in the interstellar medium," *Astrophysical Journal* **542**, p. 914, 2000.
11. P. P. Plucinsky, L. Townsley, P. S. Broos, R. J. Edgar, and S. N. Virani, "The low-energy spectral response of the acis ccds on the chandra x-ray observatory," in *High Energy Universe at Sharp Focus: Chandra Science*, E. M. Schlegel and S. D. Vrtilek, eds., p. 391, 2001.
12. M. Bautz, G. Prigozhin, M. Pivovarov, S. Jones, S. Kissel, and G. Ricker, "X-ray ccd response functions, front to back," *Nuclear Instruments and Methods A* **436**, p. 40, 1999.
13. L. K. Townsley, P. S. Broos, G. Chartas, E. Moskalenko, J. A. Nousek, and G. G. Pavlov, "Simulating ccds for the chandra advanced ccd imaging spectrometer," *Nuclear Instruments and Methods* **486**, p. 716, 2002.
14. K. A. Flanagan, C. R. Canizares, D. S. Davis, D. Dewey, J. C. Houck, and M. L. Schattenburg, "Ionization structure and the reverse shock in eo102-72," in *AIP Conf. Proc. 565: Young Supernova Remnants*, p. 226, 2001.
15. A. P. Rasmussen, E. Behar, S. M. Kahn, J. W. den Herder, and K. van der Heyden, "The x-ray spectrum of the supernova remnant 1e 0102.2-7219," *Astronomy & Astrophysics* **365**, p. L231, 2001.
16. P. Slane, Y. Chen, N. S. Schulz, F. D. Seward, J. P. Hughes, and B. M. Gaensler, "Chandra observations of the crab-like supernova remnant g21.5-0.9," *Astrophysical Journal* **533**, p. L29, 2000.
17. G. Pavlov, V. Zavlin, and D. Sanwal, "Thermal radiation from neutron stars," in *The 270-th WE-Heraeus Seminar on Neutron Stars, Pulsars and Supernova Remnants*, H. L. W. Becker and J. Truemper, eds., *MPE Report* **278**, p. 273, 2002 (astro-ph/0206024).
18. H. L. Marshall and N. S. Schulz, "Using the high-resolution x-ray spectrum of psr b0656+14 to constrain the chemical composition of the neutron star atmosphere," *Astrophysical Journal* **574**, pp. 377–381, 2002.